THE JOURNAL OF PHYSICAL CHEMISTRY C

Article

Cite This: J. Phys. Chem. C 2020, 124, 1020−1026

pubs.acs.org/JPCC

Hot-Carrier Relaxation in CdSe/CdS Core/Shell Nanoplatelets

Matthew Pelton,*[,†,‡] Yana Wang,[§] Igor Fedin,[∥,⊥] Dmitri V. Talapin,[‡,∥] and Stephen K. O'Leary[§]

[†]Department of Physics, UMBC (University of Maryland, Baltimore County), Baltimore, Maryland 21250, United States

[‡]Center for Nanoscale Materials, Argonne National Laboratory, Argonne, Illinois 60439, United States

[§]School of Engineering, The University of British Columbia, Kelowna, British Columbia V1V 1V7, Canada

[∥]Department of Chemistry and James Franck Institute, University of Chicago, Chicago, Illinois 60637, United States

ABSTRACT: We present time-resolved photoluminescence (PL) spectroscopy of a series of colloidal CdSe/CdS core/shell nanoplatelets with different core and shell thicknesses. Exciton numbers are determined from the integrated PL intensities, and carrier temperatures are determined from the high-energy exponential tail of the PL spectra. For times between 10 and 1000 ps, the measured carrier relaxation dynamics are well described by a simple model of Auger reheating: biexcitonic Auger recombination continually increases the average energy of the carriers (while decreasing their number), and this reheating sets a bottleneck to cooling through electron−phonon coupling. For times between 1 and 10 ps, the relaxation dynamics are consistent with electron−phonon coupling, where the bottleneck is now the decay of the longitudinal optical phonon population. Comparison of relaxation dynamics to recombination dynamics reveals changes in the carrier−phonon coupling for shell thicknesses greater than 4 monolayers.

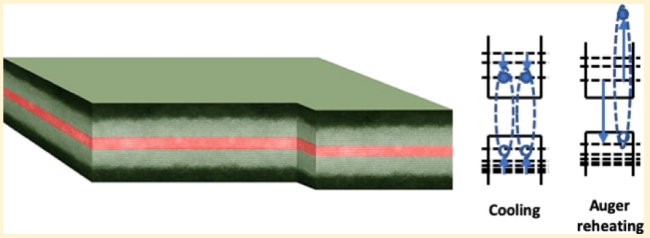

INTRODUCTION

The relaxation of carriers in semiconductor nanomaterials, from high-energy states within the conduction and valence bands down to the band-edge states, plays an important role in determining the potential optoelectronic applications of such materials. For example, rapid relaxation is favorable for light-emitting devices,[1] so that band-edge emitting states are quickly filled, and high-energy carriers are not lost to traps. On the other hand, slow relaxation is favorable for the extraction of high-energy carriers, enabling the hot carriers to be used for photocatalysis[2] or in hot carrier solar cells.[3] Relaxation dynamics are determined both by the intrinsic properties of the materials that make up the nanostructures as well as the size and shape of the nanostructures themselves. The dimensionality of the carrier confinement plays an especially important role in determining the relaxation dynamics in nanostructures; in particular, quasi-two-dimensional (quantum well) nanostructures exhibit qualitatively different carrier relaxation properties than quasi-zero-dimensional (quantum dot) nanostructures.[4]

II−VI semiconductor nanoplatelets (NPLs)[5] have properties that make them outstanding model systems for experimental studies into the relaxation dynamics in two-dimensional semiconductors.[6] Perhaps most important is that they can be synthesized colloidally with atomic-level monodispersity in their thicknesses, providing bulk samples with nearly zero inhomogeneous broadening. In addition, shells of different semiconductor materials can be grown epitaxially on NPLs using solution-phase techniques that preserve this single-monolayer (ML) monodispersity, enabling the relaxation dynamics to be probed in such heterostructures in a highly controlled manner.

We have previously examined relaxation dynamics in CdSe NPLs[7] and found that they were dominated by the effects of Auger recombination.[8] Specifically, we showed that the continuous density of states and rapid internal thermalization mean that the carrier energy distribution can be described in terms of an instantaneous temperature, $T(t)$, that decreases from a high initial value (determined by the amount of optical energy absorbed by a given NPL) to a lower temperature through an exchange of heat with the crystal lattice; this is in contrast with the sequential relaxation through discrete states that is characteristic of quantum dots.[9] However, at the same time as the carriers cool, they also undergo biexcitonic Auger recombination, which has been shown to dominate the recombination dynamics in CdSe NPLs and in CdSe/CdS core/shell NPLs.[10,11] This means that the carriers are constantly reheated at the same time as they cool: the biexcitonic Auger process involves one exciton recombining by transferring its energy to a second exciton, the excess energy of the second exciton being rapidly redistributed among the other excitons in the NPL. The competition provided by this reheating process sets the timescale of the carrier cooling.[12] The Auger reheating mechanism has also been observed to govern carrier relaxation dynamics in CdSe nanorods[13] and

Received: August 21, 2019
Revised: December 10, 2019
Published: December 11, 2019

DOI: 10.1021/acs.jpcc.9b08006
J. Phys. Chem. C 2020, 124, 1020−1026

metal halide perovskites[14−16] and is thus of broad interest in the development of optoelectronic nanomaterials.

Here, we systematically study carrier relaxation on picosecond to nanosecond timescales in CdSe/CdS core/shell NPLs over a range of core and shell thicknesses. We find that the Auger reheating mechanism dominates relaxation dynamics for timescales greater than approximately 10 ps. For shorter timescales, relaxation dynamics are dominated by phonon emission processes.

METHODS

NPL Synthesis. CdSe/CdS core/shell NPLs are synthesized as described in ref 10, following refs 17, 18. For the synthesis of 4.5 ML NPLs, we briefly degas 170 mg of cadmium myristate in 15 mL of 1-octadecene (ODE) at 80 °C in a three-necked flask and then cool the solution to room temperature. In a nitrogen glovebox (GB), we weigh out 12 mg of Se powder and add it to the degassed solution outside the GB. We then degas the resulting mixture (cadmium myristate and Se in ODE) at 90 °C for 30 min. After this, we heat up the mixture rapidly, at a rate of 20 °C per min. When the temperature reaches 190 °C and the solution turns orange-reddish, we introduce 40 mg of freshly finely ground cadmium acetate dihydrate. We continue to rapidly heat the mixture to 215 °C, at which point we lower the heating rate to let the mixture reach 240 °C without overshooting. We keep the reaction mixture at 240 °C for 5 min. Then, we cool the mixture down to 150 °C, allow it to cool down slowly to 70 °C, inject a solution of 2 mL of oleic acid in 10 mL of anhydrous hexane stored inside the GB, and allow the reaction mixture to cool down to room temperature. In the GB, we transfer the reaction mixture to a centrifuge tube and centrifuge it at 5000 rpm for 10 min (in an Eppendorf 5804 centrifuge) to isolate the NPLs from the quantum dots and other species in the solution. We collect the precipitate, disperse it in 4 mL of anhydrous hexane, and filter the solution through a 0.2 μm polytetrafluoroethylene filter.

For the synthesis of 5.5 ML NPLs, we degas 170 mg of cadmium myristate in 14 mL of ODE at room temperature. We then heat the reaction mixture under nitrogen until it reaches 240 °C and then inject 12 mg of Se powder predispersed in 1 mL of ODE by sonication. In 20 s, we introduce 60 mg of freshly finely ground $Cd(OAc)_2$ and run the reaction for 10 min. Next, we cool the reaction mixture until it reaches 80 °C and then inject 2 mL of oleic acid in 15 mL of ODE. When the suspension reaches room temperature, we centrifuge it without a nonsolvent (using an Eppendorf 5804 centrifuge) and then redisperse the NPLs in 4 mL of hexane.

We note that here we label the thicknesses of the cores as 4.5 and 5.5 ML, rather than the 4 and 5 ML identifications used in our previous publications.[7,8,10] Recent work has shown that both faces of the CdSe NPLs are terminated with Cd layers; our new labeling more accurately reflects these core thicknesses.[6]

To grow CdS shells, we first precipitate CdSe NPLs out of the stock solution with ethanol (the amount varies between 2 and 2.5 mL), centrifuge the resulting suspension at 9000 rpm for 2 min (in an Eppendorf 5804 centrifuge), discard the supernatant, and redisperse the precipitate in 4 mL of hexane. We perform two such washing cycles to remove excess Cd acetate from the synthesis.

A typical cycle of the shell growth starts with either CdSe NPLs capped with oleic acid or CdSe/CdS NPLs capped with oleylamine, dispersed in 4 mL of hexane in either case. To this solution, we add 1 mL of N-methylformamide (NMF), introduce 50 μL of 40−48% aqueous ammonium sulfide to the NMF layer, and stir the mixture for 1 min. After the complete phase transfer from hexane to NMF, we discard the hexane layer, add 4 mL of pure hexane, stir the mixture, and discard the hexane layer again. Our next step is to remove excess S^{2-} from the NMF solution of the thus formed S-capped NPLs. To the solution, we add 1 mL of acetonitrile and 1 mL of toluene to precipitate the NPLs. We centrifuge the solution at 3800 rpm for 3 min (in a Thermo Electron Corporation Centra CL2 centrifuge with a swinging rotor), discard the solution, and disperse the precipitate in 1 mL of NMF. Then, we repeat this washing procedure one more time using 5 mL of toluene as a nonsolvent. This modification to the original recipe—two washing steps after introducing S^{2-}—is essential to prevent the secondary nucleation of CdS in the next step. After the second precipitation, we redisperse the solution in 0.25 mL of NMF, introduce 1.75 mL of 0.2 M of cadmium acetate in NMF, and stir the solution for 1 min. Then, we precipitate the NPLs with 4 mL of toluene, centrifuge the suspension (as in the previous step), and redisperse the precipitate in 1 mL of NMF. To the solution, we add 4 mL of hexane and 200 μL of dried oleylamine. We stir the mixture for 1 min and centrifuge it to complete the phase separation. Secondary nucleates of CdS remain in the NMF solution. We collect the upper hexane layer with oleylamine-capped CdSe/CdS NPLs—the product of one cycle of the shell growth. We either run this solution in the next round of the shell growth or store it if it is complete. The synthesized samples are stored in ambient conditions in the dark.

Time-Resolved Photoluminescence Measurements. Measurements are also performed as described in ref 10. The NPLs are diluted in a hexane solution to the point that reabsorption of photoluminescence (PL) within the sample is negligible. The diluted sample is subsequently excited with 35 fs pump laser pulses, focused within the sample to a spot with a diameter of approximately 540 μm. The pulses are derived from an amplified Ti:sapphire laser system (Spectra-Physics Tsunami and SpitFire Pro), operating at a repetition rate of 2 kHz, and are frequency-doubled to a photon energy of 3.0 eV (wavelength of 400 nm). The PL is separated from the scattered laser light using a long-pass filter and is resolved as a function of wavelength using a grating spectrometer (Acton SP2150) and as a function of time using a streak camera with photon-counting detection (Hamamatsu C5680). All measurements are made at room temperature while stirring the samples using a magnetic stir bar in the cuvette that holds the sample. Pump-pulse fluences are determined by measuring the average power using a calibrated power meter and normalizing by the repetition rate of the laser and the measured focal area. A variable neutral density filter before the spectrometer is adjusted for each measurement to avoid the saturation of the detector. The measured PL spectra for each time delay after excitation are integrated over the range of wavelengths that corresponds to the PL peak from the NPLs in order to obtain the total PL intensity as a function of time delay. The background because of dark counts is determined by averaging over all negative time delays, and the obtained value is then subtracted from the measured data for all time delays.

DOI: 10.1021/acs.jpcc.9b08006
J. Phys. Chem. C 2020, 124, 1020−1026

Data Smoothing. Data smoothing is required to create the log−log plots used in the inversion analysis of carrier dynamics. Producing log−log plots of $-dI(t)/dt$ as a function of $I(t)$ requires the numerical differentiation of $I(t)$; if this differentiation is done directly on the experimental data, the measurement noise is amplified and this obscures the results. We therefore follow ref 20 and smooth the data by fitting them to a multiexponential function; this multiexponential fit is done simply to reduce the experimental noise and does not have any physical significance in its own right. The smoothed data are then differentiated numerically. For the log−log plots of $T(t) - T_f$ as a function of $N(t)$, numerical differentiation is not required. We therefore simply smooth the data by using a moving average filter in this case.

RESULTS

Auger-Limited Recombination Dynamics. In our previous work, we showed that biexcitonic Auger recombination dominates the recombination dynamics in CdSe NPLs and in CdSe/CdS core/shell NPLs.[10] The primary evidence for this is that the measurements of time-resolved PL are consistent with the expectation for a biexciton recombination process; that is,

$$\frac{dN(t)}{dt} = -A[N(t)]^2 \quad (1)$$

where $N(t)$ is the average number of excitons in an NPL at time t and A is a constant that determines the rate of Auger recombination, which we call the Auger recombination rate. This description, based on a continuous differential equation, has been shown to be a good approximation for $N(t) > 2$.[19]

We begin with a new analysis of time-resolved PL measurements, adapting the "inversion analysis" method of ref 20. The measured total PL intensity, $I(t)$, is proportional to $N(t)$. Accordingly, from eq 1, it is seen that a log−log plot of $-dI(t)/dt$ as a function of $I(t)$ should yield a straight line with a slope of 2. Figure 1a shows representative results; smoothing is performed as described in the Methods section. The plot is shown in terms of $N(t)$ and $-dN(t)/dt$, using the scaling between $N(t)$ and $I(t)$ based on our time-shift analysis (described below); however, this scaling affects the x- and y-axis scales equally and thus does not change the slope of the line of the corresponding log−log plot. Figure 1a also shows a fit to a straight line with a slope of 2, as is expected for biexcitonic Auger recombination dynamics; good agreement is seen for $N > 2$. Deviations are seen for $N < 1.5$; this is to be expected because at least two excitons must be present in any given NPL in order for biexcitonic Auger recombination to be possible.

The values of A obtained by this analysis can be compared to the values that we obtain by the "time-shift" analysis that we developed in refs 8, 10. In this analysis, we combine the $I(t)$ data, obtained for different excitation pump fluences, by shifting each of the traces along the time axis so that they all align with one another. At low fluences, the curves fall on top of one another without being shifted in time; this corresponds to fluences for which one or less exciton is excited, on average, in each NPL. The maximum fluence for which this is the case is used to determine the point at which the average exciton population $N(t) = 1$, and this point is used to calibrate the proportionality factor between $N(t)$ and $I(t)$.

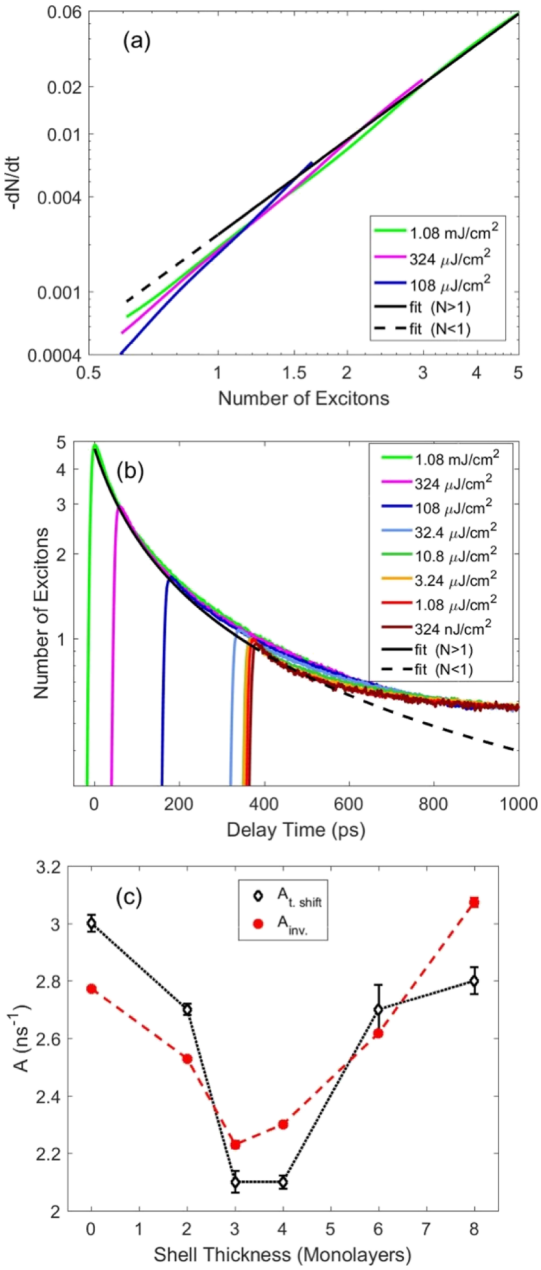

Figure 1. (a) log−log plot of the negative rate of change in the number of excitons per NPL following laser excitation, $-dN/dt$, as a function of the number of excitons, N. Data are shown for CdSe/CdS core/shell NPLs with a core thickness of 4.5 ML and a shell thickness of 4 ML, for three different excitation fluences. The fit is to a straight line with a slope of 2, as expected for a biexcitonic Auger recombination process. (b) Plot of N as a function of time after excitation, using a superset of the data considered in (a). Plots for different excitation fluences are shifted in time to give a universal decay curve. The fit is to eq 2, as expected for biexcitonic Auger recombination. (c) Values of the Auger recombination coefficient, A, obtained for NPLs with a core thickness of 4.5 ML and different shell thicknesses. Results are shown for fits of the type illustrated in (a,b).

The portion of the resulting universal decay curve corresponding to $N(t) > 1$ is then fit to the solution to eq 1:

$$N(t) = \frac{N(0)}{1 + AN(0)t} \quad (2)$$

DOI: 10.1021/acs.jpcc.9b08006
J. Phys. Chem. C 2020, 124, 1020−1026

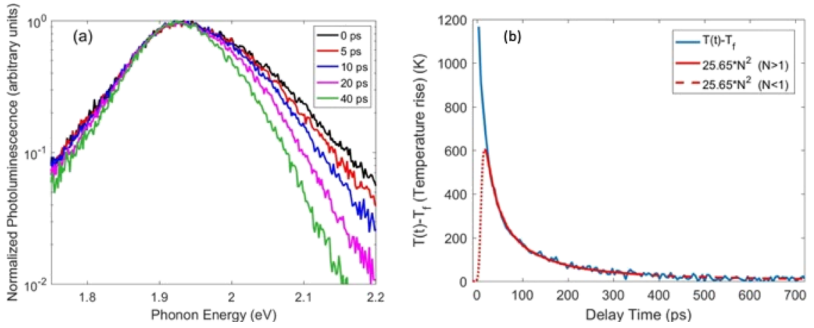

Figure 2. (a) Representative PL spectra from NPLs after excitation by a laser pulse. Data are shown for CdSe/CdS core/shell NPLs with a core thickness of 4.5 ML and a shell thickness of 4 ML. (b) Average rise in the temperature of the carriers inside the same NPLs following laser excitation, $T(t) - T_f$, as a function of time after excitation. Also plotted is the square of the average number of excitons in each NPL, N^2, scaled by a factor to make the two curves overlap at long delay times.

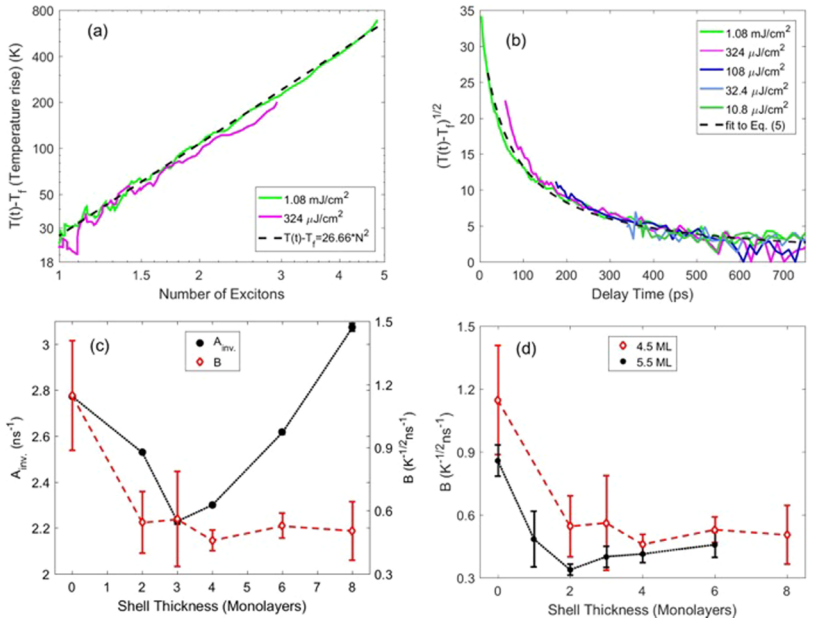

Figure 3. (a) log−log plot of the average rise in the temperature of the carriers inside NPLs following laser excitation, $T(t) - T_f$, as a function of the number of excitons. Data are shown for CdSe/CdS core/shell NPLs with a core thickness of 4.5 ML and a shell thickness of 4 ML, for two different excitation fluences. (b) Plot of $\sqrt{T(t) - T_f}$ as a function of time after excitation, using the superset of the data considered in (a). Plots for different excitation fluences are shifted in time to give a universal relaxation curve. The fit is to eq 5, as expected for a cooling process that is limited by Auger reheating. (c) Values of the Auger recombination coefficient, A, obtained for NPLs with a core thickness of 4.5 ML and different shell thicknesses (black points), compared to the values for the cooling coefficient, B, obtained for the sample NPLs (red points). (d) Values of B obtained for NPLs with different shell thicknesses, for core thicknesses of 4.5 ML (red points) and 5.5 ML (black points).

Figure 1b shows the results of this time-shift analysis and fitting for the superset of the data analyzed in Figure 1a. The only adjustable fitting parameters in this fitting method are A and $N(0)$.

The values of A obtained by this time-shift analysis are compared in Figure 1c to the values obtained by the inversion analysis. We note that the values obtained by this method correspond to those reported in ref 10; the error bars, however, are recalculated based on the fittings employed in the current analysis. The good agreement between the results of the two analyses, particularly the reproducibility of the nonmonotonic dependence of the Auger recombination rate on shell thickness,[10] validates the analytical methods employed. We note that the proportionality factor between $I(t)$ and $N(t)$ obtained from the time-shift analysis is also used for the inversion analysis. In this sense, the two analysis methods are connected; however, the effect of using a different proportionality factor would only be to change all values of A by a constant factor but would not affect their dependence on the shell thickness. The agreement between the results obtained using the two methods thus shows that the values of the Auger coefficients are reliable and are not dependent only on the details of the data analysis.

Auger-Limited Relaxation Dynamics. So far, we have verified through an independent analysis method our previous claims of Auger-dominated recombination dynamics in CdSe/CdS core/shell NPLs.[8,10] We have also previously examined the relaxation dynamics in CdSe (core-only) NPLs[7] and found that they too were dominated by the effects of Auger recombination.[8] Specifically, reheating of carriers because of Auger recombination results in a cooling bottleneck that determines the relaxation dynamics on timescales of 10−1000 ps.

DOI: 10.1021/acs.jpcc.9b08006
J. Phys. Chem. C 2020, 124, 1020−1026

Here, we examine whether Auger reheating still dominates the carrier relaxation dynamics for CdSe/CdS core/shell NPLs. The carrier temperature, $T(t)$, is obtained from the same time-dependent PL measurements as that for the exciton number, $N(t)$; in this case, however, rather than integrating the PL spectra over all wavelengths, we examine the spectra as a function of time after excitation by a laser pulse. Representative spectra are shown in Figure 2a on a log plot, showing the high-energy tails characteristic of Boltzmann distributions. Fitting these tails to a decaying exponential provides the time-dependent temperature, $T(t)$.[7,21]

This carrier temperature decays following the initial excitation, corresponding to the relaxation of carriers within the energy bands. The time dependence of this decay provides insight into the mechanisms that dominate the carrier relaxation dynamics. In the case of Auger-limited relaxation dynamics, $T(t)$ is determined by a competition between Auger reheating and electron−phonon cooling. Achermann et al. showed that this competition leads to the following temperature scaling for the carriers:[13]

$$T(t) - T_f = CN(t)^2 \tag{3}$$

where T_f is the temperature reached after the carriers and lattice have reached mutual thermal equilibrium, before the slower exchange of energy between the NPL lattice and its surroundings, and C is a constant that depends on the rate at which the carriers lose energy to phonons and the rate at which they gain energy because of Auger recombination.[13]

Figure 2b shows a plot of $T(t) - T_f$ and $CN^2(t)$ on the same graph, where C and T_f are adjusted to give the best overlap between the two curves at long times. It can be seen that there is a rapid, initial decrease in temperature that is not reflected in the exciton number dynamics. At some time, t_o, the two curves meet, and they overlap for all subsequent times.

We can also adopt an approach similar to the inversion analysis used above to analyze the recombination data, making a log−log plot of $T(t) - T_f$ as a function of $N(t)$. If Auger reheating is dominant, then the graph is expected to be a straight line with a slope of 2. The representative results are shown in Figure 3a. The expected linear relation is seen for larger values of $N(t)$. The slope of the curve increases for high $N(t)$, corresponding to the faster decay process that dominates for high exciton numbers, at short times after excitation.

The fast initial decay can also be seen by applying a time-shift analysis to the relaxation data, similar to the time-shift analysis applied above the recombination data (see Figure 1b).[8] Figure 3b shows representative results, in which the data sets for $T(t)$ have been shifted along the time axis by the same amounts as the corresponding data for $N(t)$. The shifted curves can be seen to reduce to a single, universal relaxation curve over a wide range of times, t, but there is an initial rapid decay in each curve that is not universal. That is, the initial decay depends explicitly on the time after excitation and not only on the instantaneous exciton number, $N(t)$.

To check whether Auger reheating indeed dominates the carrier dynamics after this initial rapid decay, we derive an expression for the time dependence of the carrier temperature, $T(t)$. Specifically, we combine eqs 1 and 3 to give

$$\frac{d\tau(t)}{dt} = -B[\tau(t)]^2 \tag{4}$$

where $\tau(t) = \sqrt{T(t) - T_f}$ and B is the corresponding Auger carrier relaxation rate. Solving eq 4 gives

$$\sqrt{T(t) - T_f} \propto \frac{1}{1 + B\sqrt{T(t) - T_f}\cdot(t - t_o)} \tag{5}$$

where t_o is the time at which the Auger reheating process begins. Plots of $\sqrt{T(t) - T_f}$ as a function of t show the relaxation dynamics limited by Auger reheating for timescales longer than the initial rapid decay, for all samples studied; the representative results are shown in Figure 3b.

Fits of these plots to eq 5 can be used to obtain the constant B. Because this constant depends on the competition between Auger reheating and phonon cooling, it is expected to be proportional to A and to additionally depend on the carrier−phonon coupling. Figure 3c compares the values of B obtained from the fits of eq 5 to the values of A obtained above. For shells up to 4 ML thick, these two constants are in good agreement with each other, within a scaling factor. For thicker shells, however, the two constants no longer track one another, indicating that additional factors in B that depend on electron−phonon interactions change for shell thicknesses greater than 4 ML. Similar results are obtained for NPLs with different core thicknesses (see Figure 3d).

Initial Rapid Carrier Cooling. As a final stage in our analysis of the carrier dynamics in core/shell NPLs, we isolate the initial rapid decay that occurs on timescales less than 10 ps, by taking the difference between $T(t) - T_f$ and $CN^2(t)$ in Figure 2b (and similar graphs for other samples). We fit this residual to a single exponential; only the data for the highest excitation powers provide enough points for the fits to provide reliable time constants. The time constants for the fast decay are 28 ± 2 ps for all samples, regardless of the core or shell thickness.

The measured time constant is consistent with earlier measurements in bulk CdSe,[22] where initial cooling was attributed to the generation of longitudinal optical (LO) phonons by hot carriers and the cooling rate was limited by the decay of the LO phonon population.[23,24] This model is consistent with the insensitivity of the initial decay to shell thickness, as the cooling rate depends only on the LO phonon lifetime and is largely insensitive (unlike Auger recombination[10]) to the details of the carrier wave function. This cooling stage, where the rate is limited by the LO phonon decay, is expected to occur only after a large LO phonon population has been created and is thus expected to be preceded by an even faster decay, on single-picosecond timescales, whose rate is determined by the electron−phonon coupling strength.[25] This ultrafast cooling has previously been observed using two-photon photoemission spectroscopy[25] but is beyond the time resolution of our experimental apparatus.

DISCUSSION

Although the carrier relaxation dynamics and recombination dynamics in CdSe/CdS core/shell NPLs are both dominated by the effects of Auger recombination, the proportionality constants describing the two dynamics diverge for shell thicknesses greater than 4 ML. The constant for recombination dynamics, A, depends only on the Auger recombination rate, whereas the constant for relaxation dynamics, B, also depends on electron−phonon interactions.[13] The different scaling with shell thickness thus indicates a change in these interactions.

DOI: 10.1021/acs.jpcc.9b08006
J. Phys. Chem. C 2020, 124, 1020−1026

Previous work has shown qualitative changes in the Raman scattering spectra for CdSe/CdS core/shell NPLs as the shell thickness increases.[26] In particular, CdS bulk-like modes appear in addition to interface modes, and changes in peak positions, widths, and intensities are seen with increasing shell thickness. The corresponding changes in the phonon spectral density and phonon lifetimes could account for the change in the relaxation dynamics that we observe for the thicker shells.

CONCLUSIONS

We have shown that Auger processes dominate the recombination dynamics of CdSe/CdS core/shell NPLs for all shell thicknesses and dominate the relaxation dynamics for times between 10 and 1000 ps. For shells thinner than 4 ML, the coefficients describing the recombination and relaxation dynamics track one another, indicating that they both depend only on the Auger recombination coefficient. For thicker shells, however, the coefficients diverge, indicating a change in relaxation dynamics because of changes in the phonon density of states and phonon lifetimes.[26] Quantitative, microscopic modeling of phonon properties and their effects on relaxation dynamics is a subject for future work.

We have also observed, for all CdSe/CdS core/shell NPLs studied, an initial, rapid carrier relaxation that is not limited by Auger reheating. The time constant for this relaxation is approximately 28 ps, regardless of the shell thickness, consistent with an electron−phonon cooling process whose rate is limited by the LO phonon lifetime. However, the dynamic range of the data corresponding to this initial decay was limited by the time resolution of the streak camera measurements that we performed. Further insight into this process will require time-resolved measurements with resolutions on the order of 100 fs, such as PL upconversion spectroscopy[27] or transient absorption spectroscopy.[7,28]

The results presented here complement and extend the previous measurements of carrier dynamics in colloidal semiconductor NPLs,[6] showing in particular how these dynamics are qualitatively different from those in colloidal semiconductor quantum dots. The crucial role of dimensionality is expected to hold for other quantum-confined nanomaterials. The results obtained here thus have the potential to provide broader insight into carrier recombination and relaxation in a wide array of two-dimensional nanostructures, including perovskite NPLs[29−31] and transition-metal dichalcogenides.[32,33]

AUTHOR INFORMATION

Corresponding Author

*E-mail: mpelton@umbc.edu.

ORCID

Matthew Pelton: 0000-0002-6370-8765

Dmitri V. Talapin: 0000-0002-6414-8587

Present Address

[⊥]Los Alamos National Laboratory, Los Alamos, NM 87545, U.S.A.

Author Contributions

M.P. conceived the experiment, performed streak camera measurements, and prepared the manuscript. Y.W. analyzed the data. I.F. synthesized NPL samples. D.V.T. supervised NPL synthesis. S.K.O. and M.P. supervised the data analysis. All authors contributed to discussions.

Notes

The authors declare no competing financial interest.

The Methods section is largely drawn from the Supporting Information of refs 8, 10.

ACKNOWLEDGMENTS

The authors thank Richard Schaller for assistance with the streak camera measurements. This work was performed, in part, at the Center for Nanoscale Materials, a U.S. Department of Energy Office of Science User Facility under Contract No. DE-AC02-06CH11357. Work at The University of British Columbia was funded by the Natural Sciences and Engineering Research Council of Canada. Y.W. acknowledges support from the China Scholarship Council (CSC). I.F. and D.V.T. acknowledge support from the National Science Foundation under award DMR-1629601.

REFERENCES

(1) Pietryga, J. M.; Park, Y.-S.; Lim, J.; Fidler, A. F.; Bae, W. K.; Brovelli, S.; Klimov, V. I. Spectroscopic and Device Aspects of Nanocrystal Quantum Dots. *Chem. Rev.* **2016**, *116*, 10513−10622.

(2) Harris, R. D.; Bettis Homan, S.; Kodaimati, M.; He, C.; Nepomnyashchii, A. B.; Swenson, N. K.; Lian, S.; Calzada, R.; Weiss, E. A. Electronic Processes within Quantum Dot − Molecule Complexes. *Chem. Rev.* **2016**, *116*, 12865−12919.

(3) Nozik, A. J. Quantum Dot Solar Cells. *Phys. E* **2002**, *14*, 115−120.

(4) Nozik, A. J. Spectroscopy and Hot Electron Relaxation Dynamics in Semiconductor Quantum Wells and Quantum Dots. *Annu. Rev. Phys. Chem.* **2001**, *52*, 193−231.

(5) Lhuillier, E.; Pedetti, S.; Ithurria, S.; Nadal, B.; Heuclin, H.; Dubertret, B. Two-Dimensional Colloidal Metal Chalcogenides Semiconductors: Synthesis, Spectroscopy, and Applications. *Acc. Chem. Res.* **2015**, *48*, 22−30.

(6) Pelton, M. Carrier Dynamics, Optical Gain, and Lasing with Colloidal Quantum Wells. *J. Phys. Chem. C* **2018**, *122*, 10659−10674.

(7) Pelton, M.; Ithurria, S.; Schaller, R. D.; Dolzhnikov, D. S.; Talapin, D. V. Carrier Cooling in Colloidal Quantum Wells. *Nano Lett.* **2012**, *12*, 6158−6163.

(8) Baghani, E.; O'Leary, S. K.; Fedin, I.; Talapin, D. V.; Pelton, M. Auger-Limited Carrier Recombination and Relaxation in CdSe Colloidal Quantum Wells. *J. Phys. Chem. Lett.* **2015**, *6*, 1032−1036.

(9) Klimov, V. I.; McBranch, D. W. Femtosecond 1*P*-to-1*S* Electron Relaxation in Strongly Confined Semiconductor Nanocrystals. *Phys. Rev. Lett.* **1998**, *80*, 4028−4031.

(10) Pelton, M.; Andrews, J. J.; Fedin, I.; Talapin, D. V.; Leng, H.; O'Leary, S. K. Nonmonotonic Dependence of Auger Recombination Rate on Shell Thickness for CdSe/CdS Core/Shell Nanoplatelets. *Nano Lett.* **2017**, *17*, 6900−6906.

(11) Kunneman, L. T.; Tessier, M. D.; Heuclin, H.; Dubertret, B.; Aulin, Y. V.; Grozema, F. C.; Schins, J. M.; Siebbeles, L. D. A. Bimolecular Auger Recombination of Electron-Hole Pairs in Two-Dimensional CdSe and CdSe/CdZnS Core/Shell Nanoplatelets. *J. Phys. Chem. Lett.* **2013**, *4*, 3574−3578.

(12) Borri, P.; Ceccherini, S.; Gurioli, M.; Bogani, F. Auger Heating of Carriers in Heterostructures. *Solid State Commun.* **1997**, *103*, 77−81.

(13) Achermann, M.; Bartko, A. P.; Hollingsworth, J. A.; Klimov, V. I. The Effect of Auger Heating on Intraband Carrier Relaxation in Semiconductor Quantum Rods. *Nat. Phys.* **2006**, *2*, 557−561.

(14) Li, M.; Bhaumik, S.; Goh, T. W.; Kumar, M. S.; Yantara, N.; Grätzel, M.; Mhaisalkar, S.; Mathews, N.; Sum, T. C. Slow Cooling and Highly Efficient Extraction of Hot Carriers in Colloidal Perovskite Nanocrystals. *Nat. Commun.* **2017**, *8*, 14350.

(15) Fu, J.; Xu, Q.; Han, G.; Wu, B.; Huan, C. H. A.; Look, M. L.; Sum, T. C. Hot Carrier Cooling Mechanisms in Halide Perovskites. *Nat. Commun.* **2017**, *8*, 1300.

DOI: 10.1021/acs.jpcc.9b08006
J. Phys. Chem. C 2020, 124, 1020−1026

(16) Papagiorgis, P.; Protesescu, L.; Kovalenko, M. V.; Othonos, A.; Itskos, G. Long-Lived Hot Carriers in Formamidium Lead Iodide Nanocrystals. *J. Phys. Chem. C* **2017**, *121*, 12434−12440.
(17) Ithurria, S.; Tessier, M. D.; Mahler, B.; Lobo, R. P. S. M.; Dubertret, B.; Efros, A. L. Colloidal Nanoplatelets with Two-Dimensional Electronic Structure. *Nat. Mater.* **2011**, *10*, 936−941.
(18) Ithurria, S.; Talapin, D. V. Colloidal Atomic Layer Deposition (c-ALD) using Self-Limiting Reactions at Nanocrystal Surface Coupled to Phase Transfer between Polar and Nonpolar Media. *J. Am. Chem. Soc.* **2012**, *134*, 18585−18590.
(19) Barzykin, A. V.; Tachiya, M. Stochastic Models of Charge Carrier Dynamics in Semiconducting Nanosystems. *J. Phys.: Condens. Matter* **2007**, *19*, 065105.
(20) Senty, T. R.; Cushing, S. K.; Wang, C.; Matranga, C.; Bristow, A. D. Inverting Transient Absorption Data to Determine Transfer Rates in Quantum Dot − TiO_2 Heterostructures. *J. Phys. Chem. C* **2015**, *119*, 6337−6343.
(21) Leo, K.; Rühle, W. W.; Ploog, K. Hot-Carrier Energy-Loss Rates in GaAs/$Al_xGa_{1-x}As$ Quantum Wells. *Phys. Rev. B: Condens. Matter Mater. Phys.* **1988**, *38*, 1947−1957.
(22) Junnarkar, M. R.; Alfano, R. R. Photogenerated High-Density Electron-Hole Plasma Energy Relaxation and Experimental Evidence for Rapid Expansion of the Electron-Hole Plasma in CdSe. *Phys. Rev. B: Condens. Matter Mater. Phys.* **1986**, *34*, 7045−7062.
(23) van Driel, H. M. Influence of Hot Phonons on Energy Relaxation of High-Density Carriers in Germanium. *Phys. Rev. B: Condens. Matter Mater. Phys.* **1979**, *19*, 5928−5932.
(24) Vengurlekar, A. S.; Prabhu, S. S.; Roy, S. K.; Shah, J. Large Reduction in Hot-Carrier Energy-Loss Rates in CdSe Caused by Nonequilibrium Optical Phonons. *Phys. Rev. B: Condens. Matter Mater. Phys.* **1994**, *50*, 15461−15464.
(25) Sippel, P.; Albrecht, W.; van der Bok, J. C.; Van Dijk-Moes, R. J. A.; Hannappel, T.; Eichberger, R.; Vanmaekelbergh, D. Femtosecond Cooling of Hot Electrons in CdSe Quantum-Well Platelets. *Nano Lett.* **2015**, *15*, 2409−2416.
(26) Dzhagan, V.; Milekhin, A. G.; Valakh, M. Y.; Pedetti, S.; Tessier, M.; Dubertret, B.; Zahn, D. R. T. Morphology-Induced Phonon Spectra of CdSe/CdS Nanoplatelets: Core/Shell vs. Core-Crown. *Nanoscale* **2016**, *8*, 17204−17212.
(27) Underwood, D. F.; Kippeny, T.; Rosenthal, S. J. Ultrafast Carrier Dynamics in CdSe Nanocyrstals Determined by Fluorescence Upconversion Spectroscopy. *J. Phys. Chem. B* **2001**, *105*, 436−443.
(28) Kunneman, L. T.; Schins, J. M.; Pedetti, S.; Heuclin, H.; Grozema, F. C.; Houtepen, A. J.; Dubertret, B.; Siebbeles, L. D. A. Nature and Decay Pathways of Photoexcited States in CdSe and CdSe/CdS Nanoplatelets. *Nano Lett.* **2014**, *14*, 7039−7045.
(29) Tyagi, P.; Arveson, S. M.; Tisdale, W. A. Colloidal Organohalide Perovskite Nanoplatelets Exhibiting Quantum Confinement. *J. Phys. Chem. Lett.* **2015**, *6*, 1911−1916.
(30) Bekenstein, Y.; Koscher, B. A.; Eaton, S. W.; Yang, P.; Alivisatos, A. P. Highly Luminescent Colloidal Nanoplatelets of Perovskite Cesium Lead Halide and Their Oriented Assemblies. *J. Am. Chem. Soc.* **2015**, *137*, 16008−16011.
(31) Akkerman, Q. A.; Motti, S. G.; Srimath Kandada, A. R.; Mosconi, E.; D'Innocenzo, V.; Bertoni, G.; Marras, S.; Kamino, B. A.; Miranda, L.; De Angelis, F.; et al. Solution Synthesis Approach to Colloidal Cesium Lead Halide Perovskite Nanoplatelets with Monolayer-Level Thickness Control. *J. Am. Chem. Soc.* **2016**, *138*, 1010−1016.
(32) Wang, Q. H.; Kalantar-Zadeh, K.; Kis, A.; Coleman, J. N.; Strano, M. S. Electronics and Optoelectronics of Two-Dimensional Transition Metal Dichalcogenides. *Nat. Nanotechnol.* **2012**, *7*, 699−712.
(33) Novoselov, K. S.; Mishchenko, A.; Carvalho, A.; Castro Neto, A. H. 2D Materials and van der Waals Heterostructures. *Science* **2016**, *353*, aac9439.

DOI: 10.1021/acs.jpcc.9b08006
J. Phys. Chem. C 2020, 124, 1020−1026